Effects of Polarization and Different Tissue on Terahertz Cancer Imaging

Apriono, Catur
Faculty of Engineering, Universitas Indonesia

Herry Tony Andhyka
Faculty of Engineering, Universitas Indonesia

Fitri Yuli Zulkifli
Faculty of Engineering, Universitas Indonesia

https://doi.org/10.5109/7172318

出版情報：Evergreen. 11 (1), pp.525-535, 2024-03. 九州大学グリーンテクノロジー研究教育センター
バージョン：

Effects of Polarization and Different Tissue on Terahertz Cancer Imaging

Catur Apriono[1*], Herry Tony Andhyka[1], Fitri Yuli Zulkifli[1]

[1]Faculty of Engineering, Universitas Indonesia, Indonesia

*Author to whom correspondence should be addressed:
E-mail: catur@eng.ui.ac.id

(Received October 20, 2023; Revised February 05, 2024; Accepted March 05, 2024).

Abstract: Terahertz emerges as a promising cancer imaging technique. Many factors can cause imaging results, including polarization and different tissue types. This research discusses the effect of wave polarization and different tissue types. The imaging results with perpendicularly two linear polarization give the best imaging results qualitatively and quantitatively with a standard deviation of 7.519. Different tissue types affect the imaging results, but the effect is not linear with the increasing dielectric constant. This research can be used as a consideration and reference for other researchers developing a THz imaging system.

Keywords: Cancer; Terahertz; Polarization; Tissue

1. Introduction

Cancer remains one of the most prevalent and deadly diseases affecting humanity. It has the highest mortality rate worldwide, causing approximately 10 million deaths in 2020 [1,2]. Among various types of cancer, including breast, lung, colon, prostate, and skin cancer, breast cancer is the most diagnosed. According to World Health Organization (WHO) data, breast cancer accounted for around 2.3 million new cases in 2020, ranking fifth in cancer-related deaths with approximately 685 thousand fatalities [1]. Cancer can affect anyone due to lifestyle choices, genetic predisposition, or other factors, underscoring the importance of maintaining good health and vigilance [3–5].

Discovering a definitive cure for cancer remains an ongoing challenge. While alternative methods like chemotherapy, surgery, and medications have improved and contributed to increased survival rates, they cannot guarantee a complete cure. Early cancer detection plays a crucial role in enabling effective treatment while the disease is still manageable, enhancing the chances of successful recovery. Therefore, it is vital to have reliable and safe cancer detection methods that provide high-quality imaging results. Although several technologies have been employed for cancer imaging, they each possess advantages and disadvantages and fail to fulfill both requirements mentioned earlier [6–11].

Terahertz emerges as a promising solution to address this problem. The unique characteristics of the terahertz region make it well-suited for cancer detection methods. The radiation in this frequency range is non-ionizing and poses no harm to the human body, meeting the safety requirements for cancer detection [12,13]. Moreover, terahertz technology offers high spatial resolution, translating into superior image quality, fulfilling the second requirement. The terahertz spectrum spans from 0.1 to 10 THz, falling between the millimeter wave and infrared regions on the electromagnetic spectrum [14]. A terahertz imaging system can be designed specifically for cancer detection to leverage the terahertz spectrum's advantages [15–17].

Over the years, numerous terahertz imaging techniques for cancer detection have been developed. These techniques encompass various approaches, such as mammography, pulsed systems, reflect emission, and other methodologies, targeting different types of cancer [18–24]. Several of these approaches have been dedicated to breast cancer imaging, although they may also incorporate techniques applicable to other cancer types [25–33]. However, a few designs have explored the utilization of antennas to create a distinct terahertz imaging system [34–38]. While there are challenges associated with developing antenna-based systems using terahertz frequencies, potential solutions can be implemented to optimize the performance of such systems.

Terahertz imaging system for cancer has been designed in previous research, which uses microstrip and horn antenna as the source and detector. The proposed system has been able to indicate the presence of a tumor but has not produced the best imaging results. Many factors can cause the imaging results. The placement of the transmitter and receiver antenna may affect the imaging

results. The antenna's polarization also may affect the imaging results as there is still no specific standard in this field. From the object perspective, different tissue types with different dielectric constants can also affect the imaging results as each tissue will have different absorption levels or may cause some wave incidents.

This research discusses the effect of wave polarization on imaging results. This research also discusses the effect of different tissue types on imaging results. The polarization investigation is simulated with a plane wave source with varying polarization using CST Microwave Studio. The different tissue types will be investigated by simulating imaging system scenarios on each tissue type using both plane wave and antenna sources. By observing this, hopefully, it can be used as a reference and consideration when creating a THz imaging system, especially for cancer imaging.

2. System Setup

The simulation's system scenario is built upon prior research [38]. The imaging system comprises three primary elements: the transmitter antenna, receiver antenna, and phantom model serving as the sample. The transmitter antenna is a microstrip antenna, while the receiver antenna is a horn antenna. In this configuration, a single transmitter antenna is employed as the source, while 25 receiver antennas function as detectors. The number of receiver antennas determines the level of pixel detail in the resulting imaging, generating a 5x5 image pixel resolution.

All antennas have been specifically designed for a frequency of 312 GHz, drawing upon multiple studies considered and referenced in previous research [38]. The transmitter antenna exhibits a return loss of -40 dB, accompanied by an approximate gain of 7.1 dB. As for the receiver antennas, they possess a return loss of -18 dB, along with an approximate gain of 8.1 dB. The distance between the receiver antennas and the sample is 1.5 mm. Conversely, the distance between the transmitter antenna and the sample varies across different scenarios, calculated in the subsequent section.

The sample model comprises three layers: fat, fibrous, and tumor, with a detailed description in the previous research [38]. Figure 1 illustrates the internal composition of the sample and can be utilized for comparing the imaging results with this visual representation. The red section denotes the tumor, the fibrous region by the orange section, and the fat region by the yellow section. The dimensions of the sample measure 3 mm in length, width, and height.

The transmitter antenna acting as a source will emit waves propagating through the sample [39]. The receiver antenna will then receive the propagating wave, which acts as a detector. This research considers the received power level detected by the detector by using the S21 parameter in the dB unit, which is a comparison of the received power at the receiver with the transmit power at the transmitter. The received power value from each receiver antenna will be visualized into a 2D image for the imaging results.

Fig. 1: Reference Results of the Breast Cancer Model

3. Simulation Results

3.1 Polarization Variation

Polarization variation simulation uses two sources: plane wave and antenna. The plane wave simulations use 5 different polarizations, while the antenna simulation results will be compared to the plane wave simulation. The plane wave scheme consists of a plane wave as a source, a horn antenna as a sensor, and a phantom model. The scheme used can be seen in Fig. 2. The distance between the sensor and the object is 1.5 mm. The plane wave source is on the other side of the object, with a distance of 1.5 mm from the object. Each scheme uses a plane wave with a power of 1 V/m. The scheme used is the same for the five polarization variations simulated.

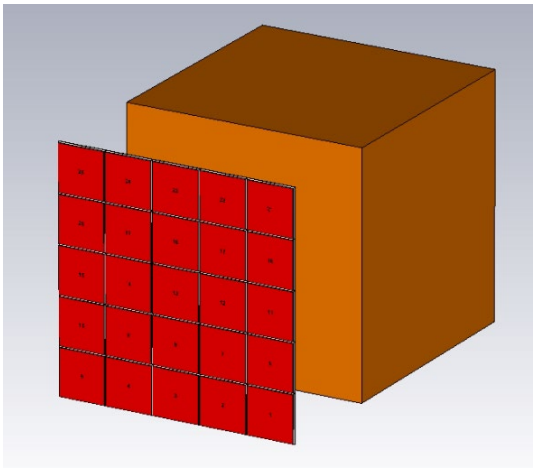

Fig. 2: Imaging Scheme for Polarization Variation with Plane Wave Source

Figure 3 shows the imaging results using linear horizontal polarization. The received power ranged from -84.071 dB to -124.660 dB.

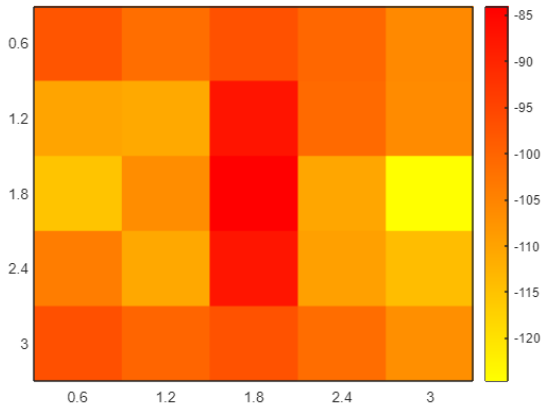

Fig. 3: Imaging Results for Linear X Polarization

Figure 4 shows the imaging results using linear vertical polarization. The received power ranged from -84.239 dB to -136.030 dB.

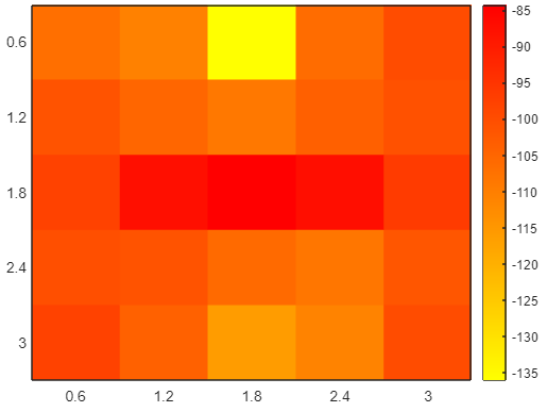

Fig. 4: Imaging Results for Linear Vertical Polarization

Figure 5 shows the imaging results using linear two polarization. The received power ranged from -78.134 dB to -116.950 dB.

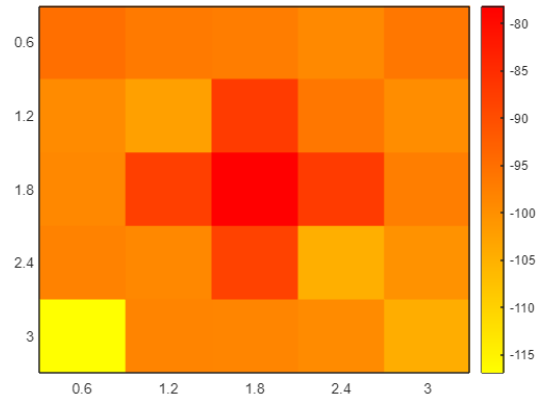

Fig. 5: Imaging Results for Linear Dual Polarization

Figure 6 shows the imaging results using left circular polarization. The received power ranged from -81.132 dB to -118.870 dB.

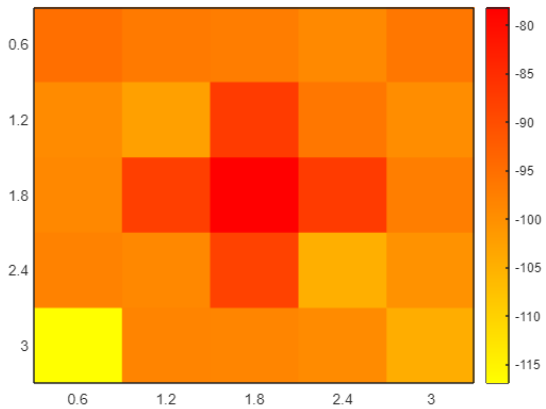

Fig. 6: Imaging Results for Left Circular Polarization

Figure 7 shows the imaging results using right circular polarization. The received power ranged from -81.156 dB to -109.070 dB.

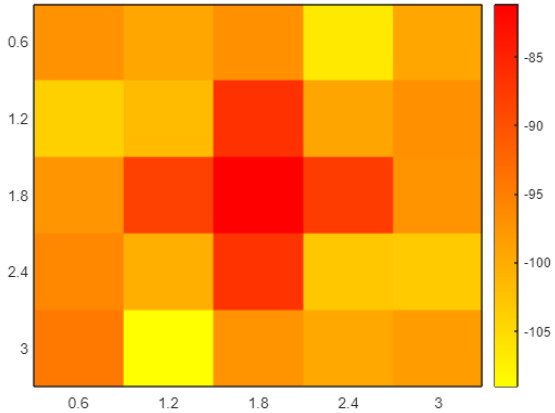

Fig. 7: Imaging Results for Right Circular Polarization

The antenna scheme consists of a transmitter antenna as a source, a 25-horn array antenna as a sensor, and a phantom model. The scheme used can be seen in Fig. 8. The distance between the sensor and the object is 1.5 mm. Figure 9 shows the imaging results using an antenna source. The received power ranged from -16.280 dB to -55.241 dB.

3.2 Tissue Type Variation

In this section, simulations are carried out with various tissue types. Three variations of tissue types are simulated using both plane wave sources and antennas. The three types of tissue are fat, fibrous, and tumor. In the previous simulations, the imaged object consisted of a combination of these 3 types of tissue.

In this simulation variation, simulations are carried out on objects that only consist of 1 type of tissue. This tissue type variation simulation is carried out to determine the phenomena that occur when waves pass through that type of tissue and how big the effect is on the waves. The distance from the source to the object is 1.5 mm. The distance from the sensor to the object is 1.5 mm. The size of the tissue-type object is 3 mm. All distances and sizes

are the same in each variation of the simulation. The plane wave scheme consists of a plane wave as a source, a horn antenna as a sensor, and a phantom model. Each scheme uses a plane wave with a power of 1 V/m.

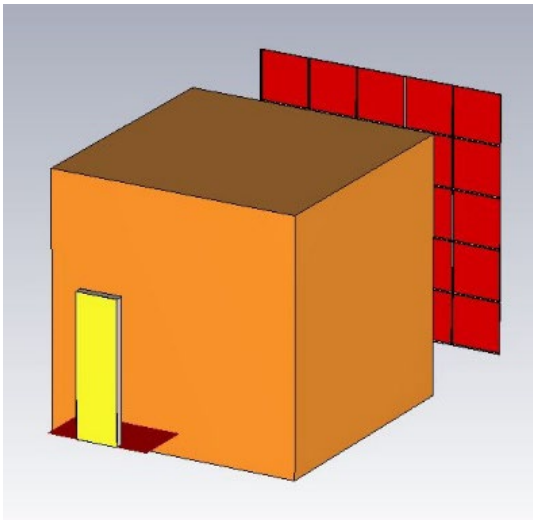

Fig. 8: Imaging Scheme for Polarization Variation with Antenna Source

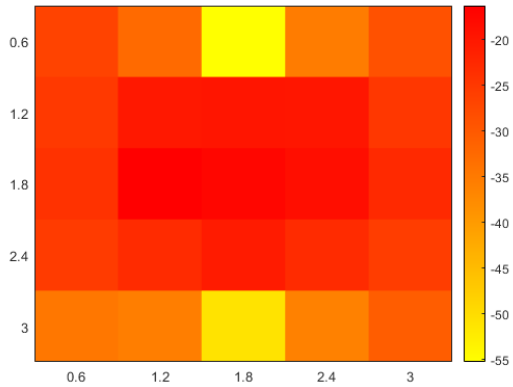

Fig. 9: Imaging Results for Antenna Scheme

Plane-wave scheme with fat tissue type can be seen in Fig. 10. The plane-wave source is on the other side of the object with a distance of 1.5 mm. The distance between the sensor and the object and the size of the object is the same as previously mentioned. Figure 11 shows the imaging results for fat tissue type using a plane wave source. The received power ranged from -83.857 dB to – 115.150 dB.

Plane-wave scheme with fibrous tissue type can be seen in Fig. 12. The plane-wave source is on the other side of the object with a distance of 1.5 mm. The distance between the sensor and the object and the size of the object is the same as previously mentioned. Figure 13 shows the imaging results for fibrous tissue type using a plane wave source. The received power ranged from -87.432 dB to – 113.700 dB.

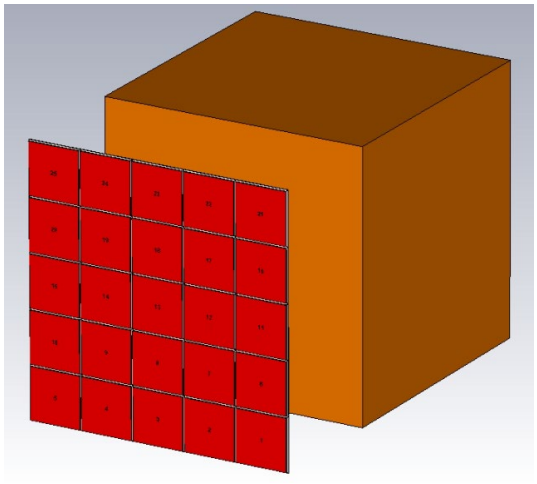

Fig. 10: Scheme for Fat Tissue Type with Plane Wave Source

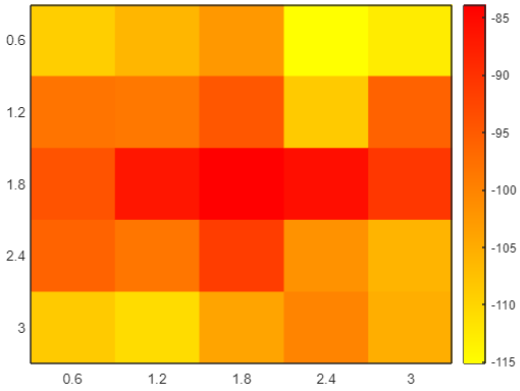

Fig. 11: Imaging Results from Fat Tissue Scheme Plane Wave Source

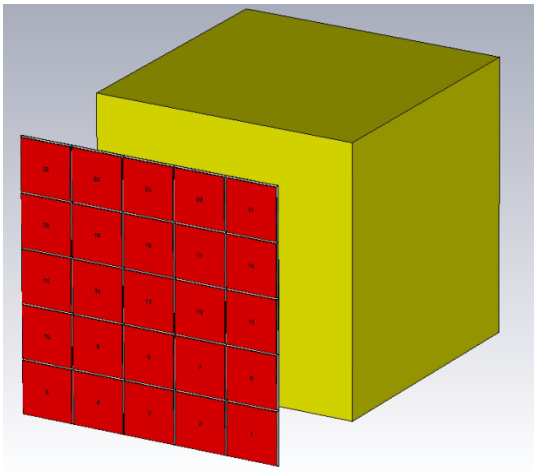

Fig. 12: Scheme for Fibrous Tissue Type with Plane Wave Source

Plane-wave scheme with tumor tissue type can be seen in Fig. 14. The plane-wave source is on the other side of the object with a distance of 1.5 mm. The distance between the sensor and the object and the size of the object is the same as previously mentioned. Figure 15 shows the imaging results using a plane wave source. The received power ranged from -86.825 dB to – 105.710 dB.

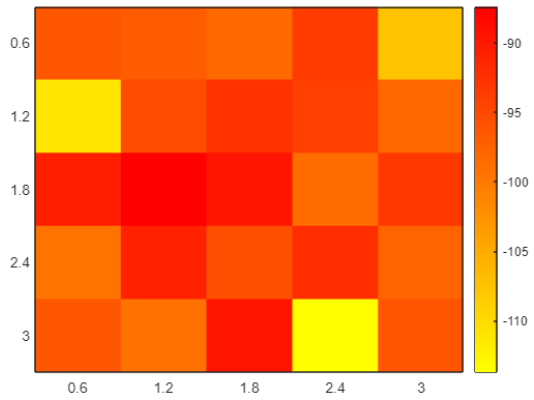

Fig. 13: Imaging Results from Fibrous Tissue Scheme Plane Wave Source

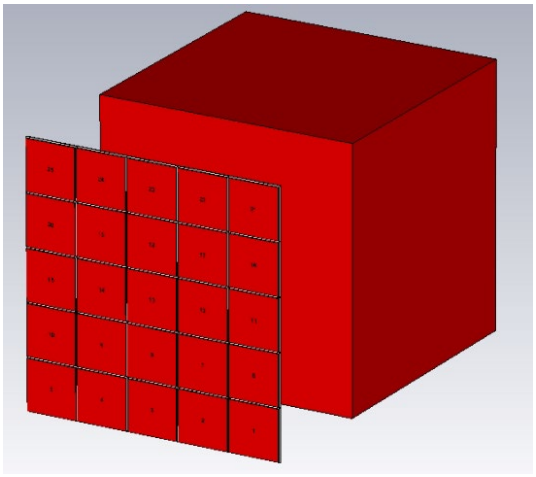

Fig. 14: Scheme for Tumor Tissue Type with Plane Wave Source

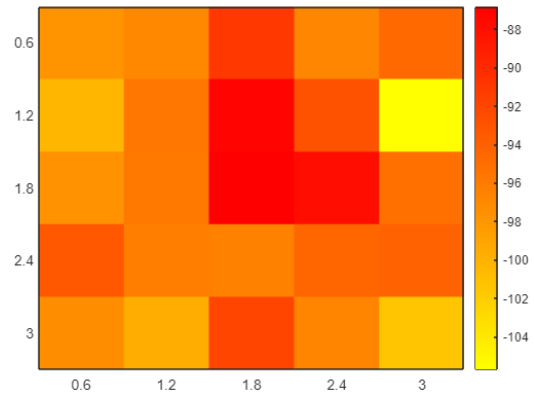

Fig. 15: Imaging Results from Tumor Tissue Scheme Plane Wave Source

The antenna scheme consists of a microstrip antenna as a source, a horn antenna as a sensor, and a phantom model. The antenna schematic with fat tissue type can be seen in Fig.16. The distance between the source and sensor with the object and the object's size is the same as previously mentioned. Figure 17 shows the imaging results for fat tissue type using an antenna source. The received power ranged from -20.107 dB to – 59.959 dB.

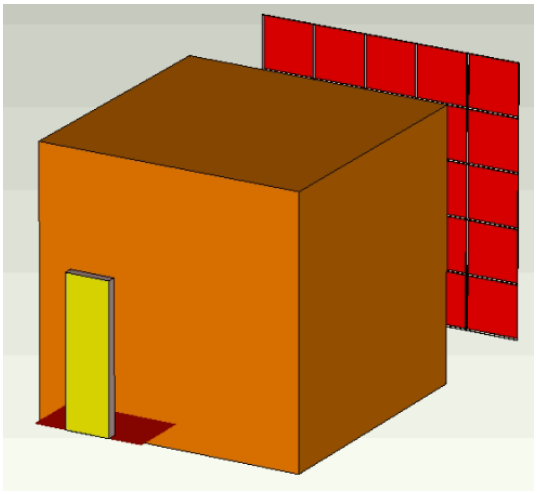

Fig. 16: Scheme for Fat Tissue Type with Antenna Source Source

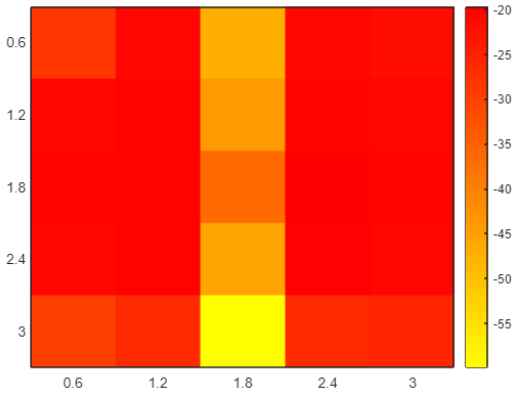

Fig. 17: Imaging Results from Fat Tissue Scheme Plane Wave Source

The antenna schematic with fibrous tissue type can be seen in Fig.18. The distance between the source and sensor with the object and the object's size is the same as previously mentioned. Figure 19 shows the imaging results for fibrous tissue type using an antenna source. The received power ranged from -19.405 dB to – 56.072 dB.

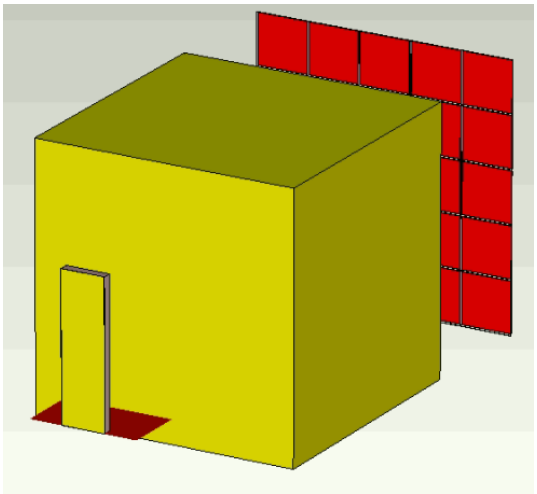

Fig. 18: Scheme for Fibrous Tissue with Antenna Source

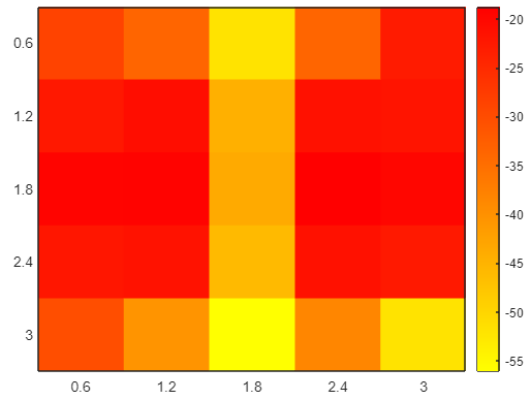

Fig. 19: Imaging Results from Fibrous Tissue Scheme Plane Wave Source

The antenna schematic with tumor tissue type can be seen in Fig. 20. The distance between the source and sensor with the object and the object's size is the same as previously mentioned. Figure 21 shows the imaging results for fibrous tissue type using an antenna source. The received power ranged from -17.498 dB to – 50.037 dB.

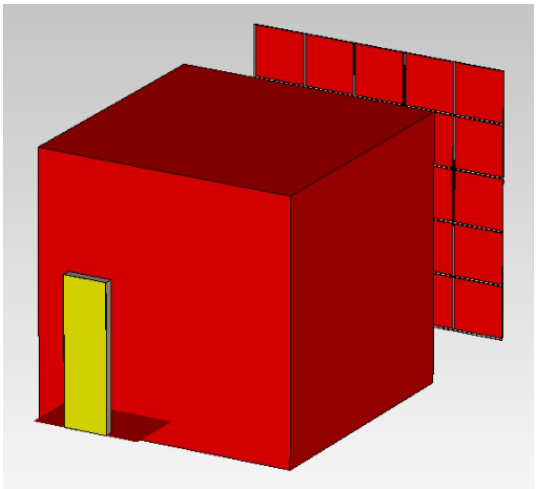

Fig. 20: Scheme for Tumor Tissue Type with Antenna Source Source

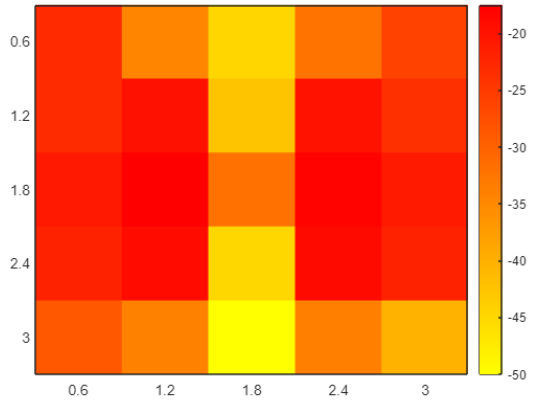

Fig. 21: Imaging Results from Tumor Tissue Scheme Plane Wave Source

4. Simulation Results

4.1 Polarization Variation Analysis

The imaging results of polarization variations with plane wave sources can be seen in Fig.3 – 7. The imaging results show that the waves' polarization affects the imaging results.

With the condition of the tumor being in the middle of the phantom, the five polarizations have different effects. On x-polarized imaging, the area of the highest value is in the center of the tumor but tends to extend more vertically. In imaging with vertical polarization, the part with the highest value is also in the middle but reverses where the highest value tends to widen towards the horizontal. A reddish color on the imaging results indicates this highest value.

Quite different things happen to the imaging results with dual polarization. The imaging results show that by combining these two polarizations, the high value is both horizontally and vertically from the center of the imaging. The imaging results with this polarization give a combined impression of the imaging results with horizontal and vertical polarization.

The results of imaging with circular polarization are observed. The two circular polarizations give almost the same results as the dual polarization, with a high value in the middle, vertically and horizontally. The difference can be seen where, in the circular polarization, there is a circular accent in the color gradation of the image. Left-hand circular polarization accents the counterclockwise rotation of results, while right-hand circular polarization accents the clockwise rotation of results.

Quantitative analysis was carried out by comparing the standard deviation values. Table 1 displays the standard deviation values of each polarization variation. Based on the standard deviation value, the scheme with the right circular polarization has the lowest standard deviation value. This condition indicates that this polarization provides ideal imaging results quantitatively compared to other polarizations.

Table 1. Standard Deviation for Polarization Variation

Polarization	Standard Deviation	Range of Received Power Level (dB)
Horizontal	8.471	-84.071 to -124.660
Vertical	9.003	-84.239 to -136.030
Dual Vertical and Horizontal	7.519	-78.134 to -116.950
Circular Left	8.026	-81.132 to -118.870
Circular Right	6.494	-81.156 to -109.070

Qualitative analysis was carried out by comparing the existing imaging results. Overall, dual linear polarization

gives better and clearer imaging results qualitatively. In the middle, the red color is the brightest and clearest compared to the surrounding colors so that it can indicate the presence and location of the tumor properly. Although circular polarization also gives similar imaging results, some accents or circular patterns make the imaging results unclear. Linear dual polarization gives the best imaging results by considering the quantitative and qualitative aspects. Although quantitatively, this polarization is not the best, the standard deviation is not too high and is the best when compared to other linear polarization.

The analysis in this section also intends to compare the imaging results using an antenna source with the imaging results using a plane wave with polarization variations. This condition is done to know the polarization of the antenna. By knowing the antenna's polarization, we can know the plane wave polarization settings for plane wave simulation in other scheme variations so that apple-to-apple comparisons can be made for later analysis.

The imaging results using a microstrip antenna are observed compared to those using a plane wave. It can be said that the imaging results using a microstrip antenna are more similar to the imaging results using a plane wave horizontal polarization. This similarity is not based on the color similarity or the overall imaging results but rather the pattern of the imaging results where it can be seen that the imaging results using a microstrip antenna produce the highest reddish values tending horizontally in the center where the pattern is similar to the plane wave polarization y imaging results. This condition also indicates that the simulation experiments using microstrip antennas are valid because it is proven by the similarity of patterns when simulated using plane waves.

In addition, the difference between the simulation results using plane waves and antennas is that the propagating waves are not perfect in simulations using antennas. If the far field is calculated from the dimensions of the transmitter antenna, the distance between the antennas is more than the far field, although only a little. In addition, the power and gain generated by the antenna and its radiation pattern make the difference in value between the simulation with the antenna and plane wave. However, if we look at the pattern, there are still similarities between the two simulations.

This analysis must be explored using other simulation variations where the tumor point is moved, not in the middle. By carrying out these variations, it can be further proven whether the analysis of the polarization effect is true or not. However, this simulation indicates that the polarization effect on the waves influences the imaging results. However, this experiment is not too significant because the five results still indicate the tumor spot is in the middle of the sample.

4.2 Tissue Type Variation Analysis

Imaging results of variations in tissue types with plane wave sources can be seen in Fig.11, Fig.13, and Fig.15. When viewed from the three imaging results. It can be said that the three types of tissue influence the waves that enter the object, resulting in various results. The assumption is that with a plane wave source that produces planar waves, the power received by each sensor will be the same. The different power levels will differentiate the three types of tissue due to the absorption of the three types of tissue with different characteristics. However, the three imaging results are quite different, and the pattern of imaging results varies widely.

A wave phenomenon occurs both inside and out of the object. This phenomenon can be analyzed from the power flow results. The power flow simulation results can be seen in Fig. 22 – 24. Figure 25 shows the power scale from the power flow results.

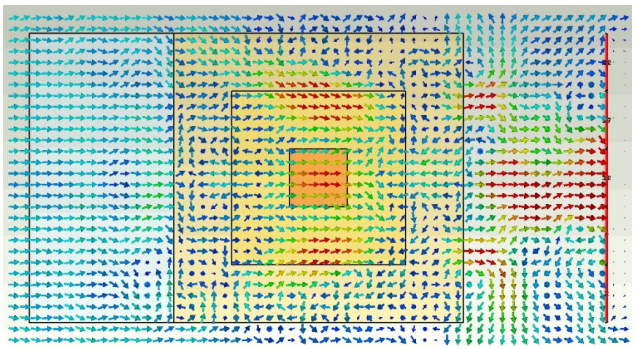

Fig. 22: Power Flow for Fat Tissue Plane Wave Source

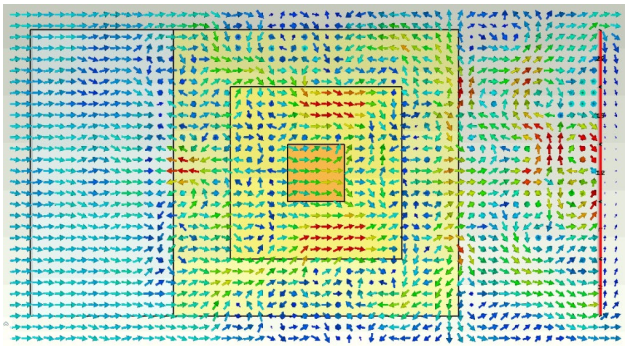

Fig. 23: Power Flow for Fibrous Tissue Plane Wave Source

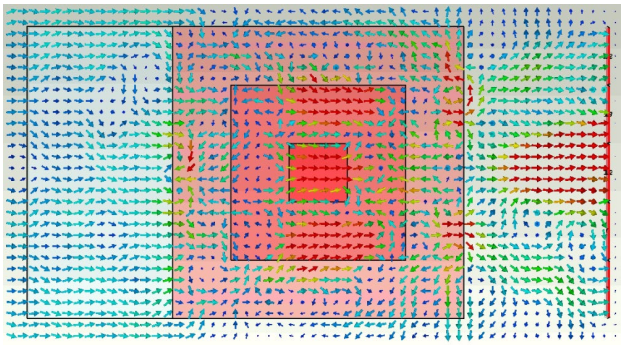

Fig. 24: Power Flow for Tumor Tissue Plane Wave Source

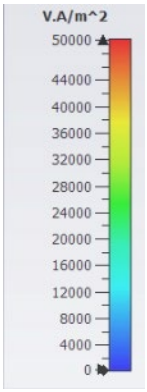

Fig. 25: Color Scale for Power Flow Results

The simulation results show the power flow from the source on the left side of the image that passes through the object and then is received by the sensor on the right side. The results displayed a two-dimensional power flow in the object's center and viewed from the side of the system. From the three power flow results, it can be seen that a phenomenon occurred.

Near the edges, some power directions tend to converge towards the center, indicating the occurrence of diffraction. Diffraction refers to the deflection of waves when they encounter an obstacle that is proportional in size to the wavelength. In this study, the frequency employed is 312 GHz, corresponding to a wavelength of approximately 960 µm or nearly 1 mm. On the other hand, the object being imaged has a size of 3 mm. Given the comparable scales of the wavelength and the object size, it is likely that diffraction phenomena occur as the waves penetrate the object.

However, the diffraction patterns are not the same as one another. In addition, the same phenomenon also occurs when waves come out of objects, namely waves that diffract and interfere with each other. However, the diffraction patterns are also not the same as one another. This phenomenon causes the imaging results to vary in the three tissue types.

Imaging results of variations in tissue type with the antenna source can be seen in Fig.17, Fig.19, and Fig. 21. When viewed from the three imaging results. It can be said that the three types of tissue influence the waves that enter the object. However, the imaging results are the same in the scheme with the antenna source.

It can be seen from the three imaging results that the center of the image is the part with the lowest power level, while the left and right are the parts with the same high power level. This condition indicates that a phenomenon occurs to produce the imaging results obtained. Quantitative analysis was carried out by comparing the standard deviation values. Table II displays the standard deviation values for each type of network.

This standard deviation indicates the population's distribution level, in the context of this study, is received power. So, it can be said that the standard deviation value describes how much the diffraction effect occurs, resulting in a wave deflection. As previously mentioned, these three tissue types have different dielectric constants: fat tissue is 2.41, fibrous is 2.8, and tumor is 3.15. Based on the standard deviation value, it was found that the increase in the dielectric constant was not proportional to the increase in the diffraction effect. Further analysis is carried out to understand the phenomena that occur in this scheme. The analysis examined these three tissue-type schemes' power flow simulation results. The power flow simulation results can be seen in Fig. 26 – 28. Fig. 25 shows the power scale from the power flow results.

Table 2. Standard Deviation for Tissue Type Variation with Antenna

Tissue Type	Standard Deviation	Range of Received Power Level (dB)
Fat	10.709	-83.857 to -115.150
Fibrous	11.906	-87.432 to -113.700
Tumor	9.592	-86.825 to -105.710

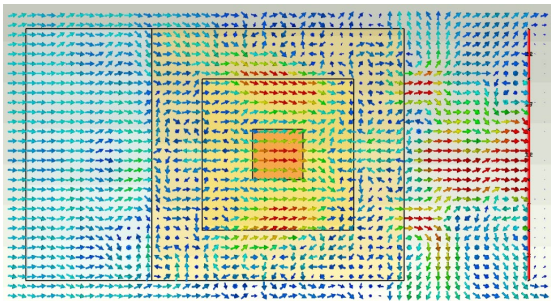

Fig. 26: Power Flow for Fat Tissue Antena Source

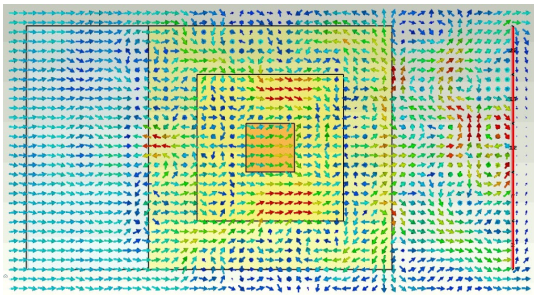

Fig. 27: Power Flow for Fibrous Tissue Antenna Source

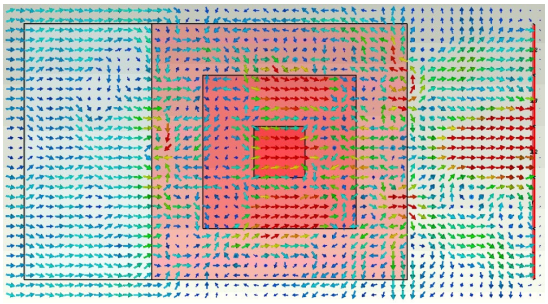

Fig. 28: Power Flow for Tumor Tissue Antenna Source

The first thing that can be seen is the phenomenon that occurs is the same as the previous scheme variations where wave diffraction occurs inside the object. However, the

diffraction effect is not noticeable when the waves leave the object. The wave that comes out of the object has quite a lot of power but weakens when it reaches the sensor. This condition causes the imaging results to be obtained where the power in the middle is weak, resulting in yellow and orange colors. Just like the simulation with a plane wave source, the simulation with an antenna source show that even when simulating an object with the same type of network, the imaging results are not uniform due to the wave incident phenomenon that occurs when the wave is inside the object.

The novelty of this research is the analysis of potential factors that affect the terahertz imaging system, especially for breast cancer imaging. This research is needed due to only a few research that observed the challenges and limitations of the terahertz imaging system. Most of the research only focuses on creating the system without giving more observation of factors that can affect the whole system.

There are a few researchers that have observed these challenges. A study has been done to analyze the challenges of imaging breast cancer due to the water content of breast tissue and constant changes in tumor size and properties [40]. Other studies observe the heating effect inside the body to the terahertz radiation or wave [41]. A study was also done to get a better understanding of the interaction between terahertz waves and breast cancer by mathematical modeling using the Double Debye Theory [42].

Table 3 shows the comparison of this research with related other research. It shows that factors of transmitter and receiver types, scanning method and polarization are also affecting the standard deviation. This research obtains a comparison with the best standard deviation by combining direct radiation and circular polarization. This method is useful to provide more practical dan faster results compared to translation scanning, which needs a longer time in data acquisition.

Table 3. Comparison with related research

Transmitter type	Detector Type	Scanning method	Polarization	Standard Deviation
Microstrip array 1D	Microstrip array 1D	translation scanning	linear	5.494[43]
Microstrip array 2D	Microstrip array 2D	translation scanning	linear	4.55 [36]
Microstrip array 1D	Horn	direct radiation	linear	12.327[44]
Plane-wave source	Horn	Direct radiation	circular	6.494 (this paper)

From those studies mentioned above, countless factors still need to be observed, and this study is observing some of the factors, which are polarization and tissue type effect. The study above also mentions the need for simulation to observe these challenges besides analysis using mathematical modeling and theory. Thus, this research is done by simulating these factors that can affect the imaging results.

5. Conclusion

This research successfully simulated different THz breast cancer imaging scenarios with polarization and tissue type variations. Based on the results, polarization affects the imaging results. Dual linear polarization gives the best imaging results qualitatively and quantitatively, with a standard deviation of 7.519. Different tissue types affect the imaging results based on the results, but the effect is not linear with the increasing dielectric constant. This research can be used as a consideration and reference for other researchers to determine the best polarization for antenna design when creating a THz imaging system. Also, this research shows that further exploration and observation need to be done to minimize the diffraction effect that may be happening due to different tissue effects.

Acknowledgments

Universitas Indonesia supports this research through the International Indexed Publication (PUTI) Postgraduate (Pascasarjana) Grant, 2023, number NKB-250/UN2.RST/HKP.05.00/2023.

References

1) J. Ferlay, M. Colombet, I. Soerjomataram, D.M. Parkin, M. Piñeros, A. Znaor, and F. Bray, "Cancer statistics for the year 2020: an overview," *Int J Cancer*, 149 (*4*) 778–789 (2021). doi:10.1002/IJC.33588.
2) H. Sung, J. Ferlay, R.L. Siegel, M. Laversanne, I. Soerjomataram, A. Jemal, and F. Bray, "Global cancer statistics 2020: globocan estimates of incidence and mortality worldwide for 36 cancers in 185 countries," *CA Cancer J Clin*, 71 (*3*) 209–249 (2021). doi:10.3322/CAAC.21660.
3) D.A. Susanto, M. Suef, and P.D. Karningsih, "Level of implementation of gmp and ssop in smes wet noodle production process with gap analysis tools," *Evergreen*, 10 (*1*) 510–518 (2023). doi:10.5109/6782155.
4) H.K. Chaudhary, K. Saraswat, H. Yadav, H. Puri, A.R. Mishra, and S.S. Chauhan, "A real time dynamic approach for management of vehicle generated traffic," *Evergreen*, 10 (*1*) 289–299 (2023). doi:10.5109/6781078.
5) P. Chankapure, P. Doggali, K. Motghare, S. Waghmare, S. Rayalu, Y. Teraoka, and N. Labhsetwar, "Coal and biomass based fuels in rural india: emissions and possibility of their control," *Journal of Novel Carbon Resource Sciences*, 4 8–12 (2011).
6) J. V. Frangioni, "New technologies for human cancer imaging," *Journal of Clinical Oncology*, 26 (*24*)

4012–4021 (2008). doi:10.1200/JCO.2007.14.3065.
7) K.E. Darras, R. Spouge, R. Hatala, S. Nicolaou, J. Hu, A. Worthington, C. Krebs, and B.B. Forster, "Integrated virtual and cadaveric dissection laboratories enhance first year medical students' anatomy experience: a pilot study," *BMC Med Educ*, 19 (*1*) 1–6 (2019). doi:10.1186/S12909-019-1806-5/TABLES/3.
8) N. Amornsiripanitch, S. Bickelhaupt, H.J. Shin, M. Dang, H. Rahbar, K. Pinker, and S.C. Partridge, "Diffusion-weighted mri for unenhanced breast cancer screening," *Radiology*, 293 (*3*) 504–520 (2019). doi:10.1148/RADIOL.2019182789.
9) J.J. Vaquero, and P. Kinahan, "Positron emission tomography: current challenges and opportunities for technological advances in clinical and preclinical imaging systems," *Https://Doi.Org/10.1146/Annurev-Bioeng-071114-040723*, 17 385–414 (2015). doi:10.1146/ANNUREV-BIOENG-071114-040723.
10) G.L. Gravina, V. Tombolini, M. Di Staso, P. Franzese, P. Bonfili, A. Gennarelli, L. Di Nicola, C. Masciocchi, and E. Di Cesare, "Advances in imaging and in non-surgical salvage treatments after radiorecurrence in prostate cancer: what does the oncologist, radiotherapist and radiologist need to know?," *Eur Radiol*, 22 (*12*) 2848–2858 (2012). doi:10.1007/s00330-012-2546-7.
11) M.M. Khalil, J.L. Tremoleda, T.B. Bayomy, and W. Gsell, "Molecular spect imaging: an overview," *Int J Mol Imaging*, 2011 1–15 (2011). doi:10.1155/2011/796025.
12) Y. Zhang, C. Wang, B. Huai, S. Wang, Y. Zhang, D. Wang, L. Rong, and Y. Zheng, "Continuous-wave thz imaging for biomedical samples," *Applied Sciences 2021, Vol. 11, Page 71*, 11 (*1*) 71 (2020). doi:10.3390/APP11010071.
13) M. Wan, J.J. Healy, and J.T. Sheridan, "Terahertz phase imaging and biomedical applications," *Opt Laser Technol*, 122 105859 (2020). doi:10.1016/J.OPTLASTEC.2019.105859.
14) J.B. Baxter, and G.W. Guglietta, "Terahertz spectroscopy," *Anal Chem*, 83 (*12*) 4342–4368 (2011). doi:10.1021/ac200907z.
15) M. Gezimati, and G. Singh, "Advances in terahertz instrumentation and technology for cancer applications," *International Conference on Infrared, Millimeter, and Terahertz Waves, IRMMW-THz*, 2022-August (2022). doi:10.1109/IRMMW-THZ50927.2022.9896072.
16) T. Skotnicki, and W. Knap, "Terahertz technologies and applications," *Proceedings of the 26th International Conference "Mixed Design of Integrated Circuits and Systems", MIXDES 2019*, 34–37 (2019). doi:10.23919/MIXDES.2019.8787160.
17) Y. He, Y. Chen, L. Zhang, S.W. Wong, and Z.N. Chen, "An overview of terahertz antennas," *China Communications*, 17 (*7*) 124–165 (2020). doi:10.23919/J.CC.2020.07.011.
18) K. Liu, Q. Sun, X. Chen, and E. Pickwell-macpherson, "Highly sensitive terahertz imaging method for paraffin embedded cancer samples," (n.d.).
19) H. Chen, T.F. Tseng, J.T. Lu, T.H. Chen, C.C. Kuo, S.C. Fu, W.J. Lee, Y.F. Tsai, Y.Y. Huang, E.Y. Chuang, Y.J. Hwang, and C.K. Sun, "High-sensitivity in vivo thz fiber-scanning mammography of early breast cancer in nude mice," *Optics InfoBase Conference Papers*, 5–6 (2011). doi:10.1364/cleo_si.2011.cthv5.
20) A. Portieri, M. Grootendorst, and T. Fitzgerald, "Intra-operative terahertz probe for detection of breast cancer," *2015 8th UK, Europe, China Millimeter Waves and THz Technology Workshop, UCMMT 2015*, 4–5 (2016). doi:10.1109/UCMMT.2015.7460611.
21) A. Shariffar, T. Bowman, C. Lai, M. Huang, M. El-Shenawee, and K. Bailey, "Modelling the interaction of thz waves with breast cancer tissues," *2018 IEEE Antennas and Propagation Society International Symposium and USNC/URSI National Radio Science Meeting, APSURSI 2018 - Proceedings*, 1843–1844 (2018). doi:10.1109/APUSNCURSINRSM.2018.8609091.
22) T. Bowman, M. El-Shenawee, and K. Bailey, "Terahertz imaging of transgenic murine breast cancer tumors," *2018 IEEE Antennas and Propagation Society International Symposium and USNC/URSI National Radio Science Meeting, APSURSI 2018 - Proceedings*, 901–902 (2018). doi:10.1109/APUSNCURSINRSM.2018.8609230.
23) H. Sumarti, S.R. Anggita, F.R. Pratama, and A.N. Tasyakuranti, "Texture-based classification of benign and malignant mammography images using weka machine learning : an optimal approach," *Evergreen Journal*, 10 (*03*) 1570–1580 (2023). doi.org/10.5109/7151705
24) A. Yussupov, and R.Z. Suleimenova, "Use of remote sensing data for environmental monitoring of desertification," *Evergreen Journal*, 10 (*1*) 300–307 (2023). doi:10.5109/6781080.
25) M. Boutaayamou, D. Cerica, and J.G. Verly, "Terahertz pulsed imaging of dehydrated human breast cancer samples," *International Conference on Infrared, Millimeter, and Terahertz Waves, IRMMW-THz*, 2020-November 65–66 (2020). doi:10.1109/IRMMW-THZ46771.2020.9370383.
26) T. Chavez, N. Vohra, J. Wu, M. El-Shenawee, and K. Bailey, "Spatial image segmentation for breast cancer detection in terahertz imaging," *2020 IEEE International Symposium on Antennas and Propagation and North American Radio Science Meeting, IEEECONF 2020 - Proceedings*, 1157–1158 (2020). doi:10.1109/IEEECONF35879.2020.9330445.
27) P. Kaurav, S. Koul, and A. Basu, "Design of sub-

terahertz waveguide iris probe for breast cancer tumor margin assessment," *2021 IEEE MTT-S International Microwave and RF Conference, IMARC 2021*, (2021). doi:10.1109/IMARC49196.2021.9714693.

28) N. Vohra, T. Bowman, M. El-Shenawee, and K. Bailey, "Image reconstruction of freshly excised human breast tumors using terahertz electrical properties," *2019 IEEE International Symposium on Antennas and Propagation and USNC-URSI Radio Science Meeting, APSURSI 2019 - Proceedings*, 571–572 (2019). doi:10.1109/APUSNCURSINRSM.2019.8888949.
29) C. Oldfield, T. Bowman, and M. El-Shcnawcc, "Development of tunable breast tissue phantoms for terahertz imaging," *2018 IEEE Antennas and Propagation Society International Symposium and USNC/URSI National Radio Science Meeting, APSURSI 2018 - Proceedings*, 1397–1398 (2018). doi:10.1109/APUSNCURSINRSM.2018.8608493.
30) N. Vohra, M. El-Shenawee, and K. Bailey, "Dehydration approach for enhancing terahertz detection of cancer in freshly excised breast tumors," *2020 IEEE International Symposium on Antennas and Propagation and North American Radio Science Meeting, IEEECONF 2020 - Proceedings*, 43–44 (2020). doi:10.1109/IEEECONF35879.2020.9330034.
31) T. Bowman, M. El-Shenawee, and K. Bailey, "Terahertz time-domain pulsed spectroscopy of human breast cancer tissues," *2018 IEEE Antennas and Propagation Society International Symposium and USNC/URSI National Radio Science Meeting, APSURSI 2018 - Proceedings*, 1067–1068 (2018). doi:10.1109/APUSNCURSINRSM.2018.8608929.
32) N. Vohra, M. El-Shenawee, and K. Bailey, "Terahertz imaging of enu injected sprague dawley rat breast cancer tumors," *2021 IEEE International Symposium on Antennas and Propagation and North American Radio Science Meeting, APS/URSI 2021 - Proceedings*, 585–586 (2021). doi:10.1109/APS/URSI47566.2021.9703938.
33) N. Vohra, T. Chavez, J.R. Troncoso, N. Rajaram, J. Wu, K. Bailey, and M. El-Shenawee, "Terahertz imaging of breast cancer using human and animal models," *2021 IEEE Conference on Antenna Measurements and Applications, CAMA 2021*, 368–371 (2021). doi:10.1109/CAMA49227.2021.9703666.
34) I. Nurfitri, and C. Apriono, "Rectangular Linear Array Microstrip Antenna Design for Terahertz Imaging," in: 2019 International Conference on Information and Communications Technology (ICOIACT), 2019: pp. 719–722. doi:10.1109/ICOIACT46704.2019.8938556.
35) M.V. Hidayat, and C. Apriono, "Design of 0.312 THz microstrip linear array antenna for breast cancer imaging application," in: 2018 International Conference on Signals and Systems, ICSigSys 2018 - Proceedings, Institute of Electrical and Electronics Engineers Inc., 2018: pp. 224–228. doi:10.1109/ICSIGSYS.2018.8372671.
36) I. Nurfitri, and C. Apriono, "Radiation Beamwidth Characterization to Enhance Terahertz Imaging Quality for Cancer Detection," in: Proceedings - CAMA 2019: IEEE International Conference on Antenna Measurements and Applications, Institute of Electrical and Electronics Engineers Inc., 2019: pp. 207–209. doi:10.1109/CAMA47423.2019.8959591.
37) H.T. Andhyka, and C. Apriono, "Design of thz high-resistivity silicon-based microstrip antenna for breast cancer imaging," *Int J Adv Sci Eng Inf Technol*, 10 (*6*) 2640–2648 (2020). doi:10.18517/ijaseit.10.6.12887.
38) H.T. Andhyka, C. Apriono, and F.Y. Zulkifli, "Terahertz imaging simulation using silicon-based microstrip antenna and horn antenna for breast cancer detection," *Jurnal Ilmiah Teknik Elektro Komputer Dan Informatika*, 8 (*4*) 520–536 (2022). doi:10.26555/JITEKI.V8I4.24809.
39) P. Ranjan, S. Yadav, H. Gupta, and A. Bage, "Design and development of machine learning assisted cylindrical dielectric resonator antenna," *Evergreen*, 10 (*1*) 308–316 (2023). doi:10.5109/6781085.
40) T. Bowman, M. El-Shenawee, and K. Bailey, "Challenges in terahertz imaging of freshly excised human breast tumors," *2018 IEEE Antennas and Propagation Society International Symposium and USNC/URSI National Radio Science Meeting, APSURSI 2018 - Proceedings*, 13–14 (2018). doi:10.1109/APUSNCURSINRSM.2018.8608576.
41) S. Ganesan, and P.K. Yalavarthy, "Modeling of terahertz heating effects in realistic tissues," *IEEE Journal on Selected Topics in Quantum Electronics*, 19 (*1*) 74–81 (2013). doi:10.1109/JSTQE.2012.2208180.
42) A. Shariffar, T. Bowman, C. Lai, M. Huang, M. El-Shenawee, and K. Bailey, "Modelling the interaction of thz waves with breast cancer tissues," *2018 IEEE Antennas and Propagation Society International Symposium and USNC/URSI National Radio Science Meeting, APSURSI 2018 - Proceedings*, 1843–1844 (2018). doi:10.1109/APUSNCURSINRSM.2018.8609091.
43) C. Apriono, and M.V. Hidayat, "Distance investigation between two linear array microstrip antenna for terahertz breast cancer imaging," in: AIP Conf Proc, AIP Publishing, 2021.
44) H.T. Andhyka, C. Apriono, and F.Y. Zulkifli, "Terahertz Propagation Investigation of Terahertz Imaging on A Cancer Object," in: 2023 International Conference on Radar, Antenna, Microwave, Electronics, and Telecommunications (ICRAMET), 2023: pp. 353–356. doi:10.1109/ICRAMET60171.2023.10366749.